ACS APPLIED BIO MATERIALS

www.acsabm.org Article

Photosystem I Enhances the Efficiency of a Natural, Gel-Based Dye-Sensitized Solar Cell

Joshua M. Passantino, Kody D. Wolfe, Keiann T. Simon, David E. Cliffel, and G. Kane Jennings*

Cite This: *ACS Appl. Bio Mater.* 2020, 3, 4465−4473 Read Online

ACCESS | Metrics & More | Article Recommendations | Supporting Information

ABSTRACT: The photosystem I (PSI) protein complex is known to enhance bioelectrode performance for many liquid-based photoelectrochemical cells. A hydrogel as electrolyte media allows for simpler fabrication of more robust and practical solar cells in comparison to liquid-based devices. This paper reports a natural, gel-based dye-sensitized solar cell that integrates PSI to improve device efficiency. TiO_2-coated FTO slides, dyed by blackberry anthocyanin, act as a photoanode, while a film of PSI deposited onto copper comprises the photocathode. Ascorbic acid (AscH) and 2,6-dichlorophenolindophenol (DCPIP) are the redox mediator couple inside an agarose hydrogel, enabling PSI to produce excess oxidized species near the cathode to improve device performance. A comparison of performance at low pH and neutral pH was performed to test the pH-dependent properties of the AscH/DCPIP couple. Devices at neutral pH performed better than those at lower pH. The PSI film enhanced photovoltage by 75 mV to a total photovoltage of 0.45 V per device and provided a mediator concentration-dependent photocurrent enhancement over non-PSI devices, reaching an instantaneous power conversion efficiency of 0.30% compared to 0.18% without PSI, a 1.67-fold increase. At steady state, power conversion efficiencies for devices with and without PSI were 0.042 and 0.028%, respectively.

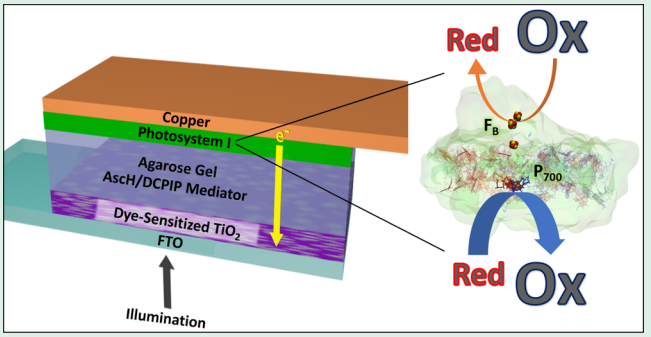

KEYWORDS: *Photosystem I, solar cell, biophotovoltaics, dye-sensitized solar cells, electrochemistry, renewable, gel electrolyte, two-electrode*

Downloaded via VANDERBILT UNIV on December 20, 2021 at 20:21:47 (UTC).
See https://pubs.acs.org/sharingguidelines for options on how to legitimately share published articles.

INTRODUCTION

The current state of solar energy conversion relies on devices with nonrenewable components, unsustainable processing, and unfavorable cost-to-efficiency ratios.[1,2] To resolve these issues, biological materials that efficiently harness the power of the sun are being explored.[3] Photoactive biological materials mass produced by nature are prospective components to drive down monetary and energy costs in photovoltaic devices. The photosynthetic protein photosystem I (PSI) found in green plants, algae, and cyanobacteria is a promising candidate for solar energy conversion. The complex attains one of the most negative reduction potentials (−0.59 V vs SHE) in nature, produces a 1.1 V difference across the thylakoid membrane, and achieves near-perfect internal quantum efficiency.[4]

PSI is known to improve the photoelectrochemical performance of many electrode materials under various conditions.[5−11] Photoelectrochemical investigations of PSI have commonly used a three-electrode liquid cell to enable a focused study of the photoelectrochemical interface between PSI and a single electrode.[10,12,13] In contrast, fewer researchers have reported the use of PSI in a two-electrode solar cell,[13−20] and most of these include solid-state devices.[14−16,19,20] Solid-state devices with PSI depend on direct electron transfer from electrodes or conducting materials to and from the P_{700} and F_B sites, which complicates device fabrication in comparison to devices dependent on mediated electron transfer (MET). Alternatively, liquid cells rely on MET, in which redox reactions occur throughout a protein film as reactants freely diffuse to the electrodes.[21]

The dye-sensitized solar cell (DSSC) is a promising, liquid-based technology that is able to mimic photosynthesis and produce robust solar conversion efficiencies.[22] Traditionally, high-performing DSSC's rely on an iodide/triiodide (I^-/I_3^-) mediator in acetonitrile with a ruthenium-based dye to sensitize the electrode.[13] Issues with the traditional high-performance devices are the toxicity and high volatility of organic solvents as well as the high cost for the ruthenium-based dyes.[22,23] PSI has been explored as a way to boost DSSC performance and, in some cases, as a way to improve renewability and cost-effectiveness. PSI has provided improvement when used as a dye-sensitizer[5,24] and as a redox film on a blackberry dye-sensitized TiO_2 electrode.[25] In these investigations, PSI was deposited onto TiO_2 to boost anode

Received: April 20, 2020
Accepted: May 28, 2020
Published: May 28, 2020

ACS Publications © 2020 American Chemical Society

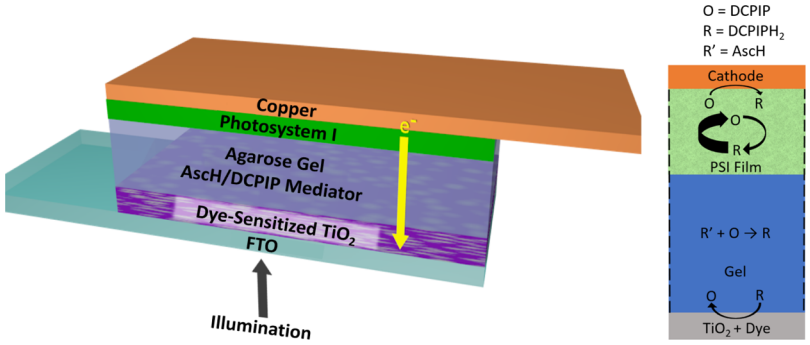

Figure 1. Schematic of biohybrid DSSC and suggested redox pathway.

performance, but using PSI to boost cathode performance while being paired with a dye-sensitized anode has not been previously explored.

Along with three-electrode investigations, PSI performance has been measured in two-electrode photoelectrochemical devices or "wet" cells. PSI films have been used to form a photobioelectrode in a device with electrolyte mediators such as Cyt c_{553}[17] and the ascorbic acid (AscH)/2,6-dichlorophenolindophenol (DCPIP) couple.[26] Additionally, PSI on gold improved performance with a copper/ITO counter electrode in an AscH/DCPIP mediator. The cell showed consistent performance over 280 days but did not reach above 0.001% external efficiency and required refilling of the liquid electrolyte.[27] PSI also enhanced a traditional I^-/I_3^- DSSC with a Pt/FTO counter electrode, boosting efficiencies from 0.24 to 0.47% when PSI was used as a macromolecular dye in TiO_2.[5]

Despite these successes, liquids are disadvantageous as electrolyte media in photovoltaic systems because of portability issues and continual maintenance resulting from leakage, evaporation, or sealant failure.[28] A quasi-solid-state gel medium negates the limitations prevalent in liquid cells while also providing similar transport capabilities for redox species. A gel analogue of a DSSC with an I^-/I_3^- mediator exhibited improved photocurrent stability after 125 days of operation versus an equivalent liquid cell.[29] These advantages allow for the minimization of evaporation and enhanced portability while still harnessing MET.

Device Design. The goal for this investigation is to design a low-cost, renewable photovoltaic device that integrates a DSSC electrode with a gel-based medium and a PSI-coated cathode to elevate the performance of the cell, as measured via the short circuit current, open circuit photovoltage, and power output. Figure 1 shows a schematic of the gel-based biohybrid solar cell. The device utilizes an FTO-coated glass slide as a transparent current collector upon which the TiO_2 film is spin-coated, annealed, and loaded with anthocyanin dye. The gel media are 0.5% wt agarose hydrogel with a supporting electrolyte and an AscH/DCPIP mediator.

Agarose is a naturally derived polysaccharide that is a principal component of agar, a gel commonly used for gel electrophoresis. Agarose has been used in DSSCs and has shown performance enhancement over equivalent liquid cells.[30,31] Agarose can form a polymer matrix in an aqueous solution while maintaining similar ionic conductivity and negating environmental hazards introduced in other types of media.[31] The use of agarose here allows for simple addition of redox mediators to customize the internal environment of the cell. Badura et al. confined PSI in a thin cross-linked Os-based redox hydrogel film of allylamine and vinylimidazole on a gold electrode in an aqueous three-electrode system purged with O_2 and a methyl viologen (MV) mediator to improve the performance of immobilized PSI.[32] The success with the redox hydrogel system proves that PSI can function well in a gel, but the use of an organic chemical for the media, a precious metal electrode, and a toxic mediator suggest challenges in renewable scale-up.

PSI has been shown to increase photovoltage from 220 mV to over 500 mV when deposited atop a TiO_2 anode in a three-electrode cell using a $[Fe(CN)_6]^{4-/3-}$ mediator couple. The improvement was attributed to PSI reducing $Fe(CN)_6^{3-}$ faster than it can oxidize $Fe(CN)_6^{4-}$ to create a higher concentration of the reduced species near the mesoporous anode, which effectively reduces charge recombination.[25] PSI is also known to produce the opposite kinetic asymmetry when exposed to the natural mediator couple AscH/DCPIP by more rapidly producing the oxidized form of DCPIP.[33] This asymmetry implies that the oxidized form of DCPIP would accumulate within the vicinity of the PSI/electrode interface, benefitting cathode performance. The opposite kinetic asymmetry for the $[Fe(CN)_6]^{4-/3-}$ and AscH/DCPIP mediator couples stems from the half-wave potentials ($E_{1/2}$) being closer to either the reduction potential for the F_B or P_{700} reaction sites.

For this investigation, three mediator systems—AscH/DCPIP, MV, and $[Fe(CN)_6]^{4-/3-}$—were assessed via photochronoamperometry (PCA) as they are commonly used in PSI-integrated electrochemical investigations because they are good donors or acceptors with the P_{700} and F_B sites of PSI.[9,21,33−36] MV is an oxygen scavenger and can rapidly accept electrons from the F_B site of PSI, creating an excess of reduced species near the cathode, which reduced the performance of this device. In the case of $[Fe(CN)_6]^{4-/3-}$, $Fe(CN)_6^{4-}$ is a slow donor to P_{700}, while $Fe(CN)_6^{3-}$ can quickly accept electrons from F_B, leading to an excess of reduced species.[37] In contrast to the reactions of MV and $[Fe(CN)_6]^{4-/3-}$ with PSI, the AscH/DCPIP mediator system is known to rapidly reduce P_{700}, causing an excess of oxidized species in solution.[33] The AscH/DCPIP couple enhances current compared to the other mediators when PSI is deposited onto the cathode (Figure S1). Some photocurrent is present in the supporting electrolyte (KCl) control. This photocurrent is attributed to water and oxygen reacting within the system, but this contribution to current is small (<5 $\mu A/cm^2$), in comparison to the overall current with AscH/DCPIP.[38]

AscH, commonly known as vitamin C, is an abundant, nontoxic molecule that protects PSI from harmful reactive oxygen species in vivo[39,40] while DCPIP is a natural, nontoxic

https://dx.doi.org/10.1021/acsabm.0c00446
ACS Appl. Bio Mater. 2020, 3, 4465−4473

redox dye commonly used as a Hill reagent. Together, they are an efficient redox couple when paired with PSI.[41] The reaction between AscH and DCPIP is a catalytic electron transfer/homogenous chemical (EC′) coupled reaction that catalytically generates reduced species.[42] Having an excess of AscH serves to increase the concentration of $DCPIPH_2$ species in the cell by continually reducing DCPIP that is not reacted at the cathode. A schematic of the AscH/DCPIP mediator system with PSI is shown in Figure S2.[43,44] As reported herein, PSI can increase photocurrent at low mediator concentrations by converting the $DCPIPH_2$ back to DCPIP near the cathode, yielding a higher rate of reduction and increasing the performance of the cell. The reaction kinetics for the AscH/DCPIP reaction mechanism are pH dependent, prompting a comparison of cell performance at different pH values.[45]

The placement of PSI on either the cathode or the anode was examined, with the observation that depositing a 4 μm thick, randomly oriented PSI film (thickness confirmed by profilometry, Figure S3) on the cathode provided enhancement while placing the film on the anode showed no improvement. PM-IRRAS spectra (Figure S4) were collected to verify the deposition of PSI onto the copper cathode. The IR spectra of a 4 μm thick PSI film show the presence of the characteristic Amide I and Amide II peaks at 1662 and 1545 cm^{-1}, respectively.[46] These results are consistent with the deposition of structurally intact PSI films on the copper cathode.

Copper was chosen as a suitable, inexpensive cathode because it has inherent energetic synergy with PSI and a substantial potential difference with the conduction band of TiO_2 (0.34 and −0.30 V vs SHE).[42] In nature, the oxidizing end of PSI, the P_{700} site, accepts electrons from the copper-containing protein plastocyanin. TiO_2 was selected as the semiconductor anode because it has a favorable energy band alignment with PSI and copper,[5] it absorbs UV light well, and it can be deposited as mesoporous films that can be sensitized with dyes to enhance light absorbance in the visible spectrum.[25] Anthocyanin (AC), a naturally occurring dye derived from blackberries, is used to sensitize TiO_2 here because it absorbs light in the 500−650 nm wavelength range, complementing the absorbance of both TiO_2 and PSI. PSI absorbs strongly in 400−500 nm and 650−700 nm wavelengths of visible light while TiO_2 absorbs strongly at <400 nm.[25] The TiO_2 and AC anodes on FTO allow light at wavelengths complementary to PSI to pass through. The extracted dye consists of approximately 90 wt % cyanidin-3-glucoside and 10 wt % cyanidin-3-glucosyl-malonate.[25]

As dye-sensitized TiO_2 is known to be a good photoanode,[5,25,29,47,48] we focus here on improving copper cathode performance. We hypothesize that by using the naturally occurring mediator couple AscH/DCPIP, we can harness the kinetic asymmetry of PSI's redox capabilities and increase photocurrent with a PSI multilayer film deposited on the cathode of a photovoltaic device. Combining these materials, we report a PSI-derived natural DSSC, and we investigate the effect of PSI film thickness, pH, and mediator concentration on the performance of the cell.

RESULTS AND DISCUSSION

Device Performance. The effect of PSI on cell photovoltage and photocurrent over a range of mediator concentrations was examined. Additionally, devices were tested at two different pH ranges: low (2.5−3.5) and neutral (6.5−7.5). The pH-dependent mole fraction of the oxidized forms of DCPIP, as described by the Henderson−Hasselbach equation, with pK_a's of 0.5 and 5.6 is shown in Figure 2, denoted as

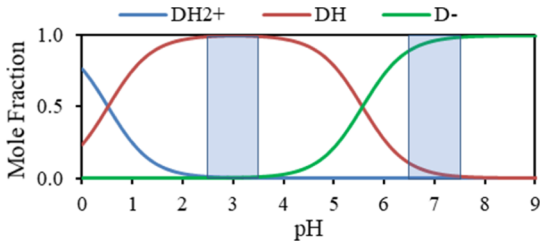

Figure 2. Mole fraction for pH-dependent forms of DCPIP. Shaded sections represent values in which devices were tested.

DH_2^+, DH, and D^-.[45] At the lower pH range, DH is the dominant oxidized form while at neutral pH, D^- is the dominant form, and these forms behave differently in electrochemical cells, with D^- providing greater current during cyclic voltammetry (Figure S5). A similar trend in activity versus pH was also observed by Petrova et al.[44] Additionally, D^- reacts with AscH at a kinetic rate that is 2 orders of magnitude slower than that for DH with AscH.[45] The overall reduction of the oxidized forms of DCPIP to $DCPIPH_2$ occurs at all pH values, but the rate of reduction is pH dependent.[45]

An advantage of a two-electrode device is that it enables the measurement of the photovoltage produced across the cell instead of examining the potential of only the working electrode that constrains three-electrode experiments. Figure 3a shows the photovoltage generated by the devices at all

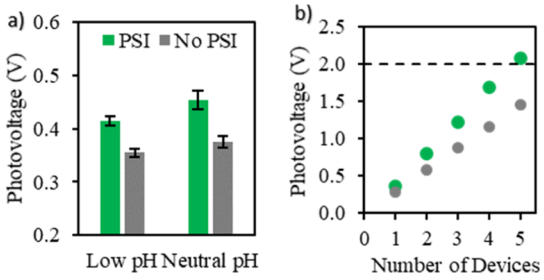

Figure 3. (a) Single-device photovoltage enhancement with PSI at low pH (2.5−3.5) and neutral pH (6.5−7.5). (b) Enhancement of photovoltage after connecting multiple devices at low pH in series.

concentrations and each pH range. For a Nernstian equilibrium process, the potential of an electrode is dependent on the ratio of the concentration of oxidized to reduced species near the electrode and is therefore independent of bulk concentration as shown in the Nernst Equation:

$$E(t) = E_0 + \frac{RT}{nF} \ln \frac{C_O(0, t)}{C_R(0, t)} \quad (1)$$

Devices without PSI produce photovoltages of 0.35 and 0.37 V at low pH and neutral pH values, respectively, while the addition of a PSI film increases the photovoltage at each pH range. We expect that the faster reaction between PSI's $P700^+$ and $DCPIPH_2$ versus that between F_B^- and DCPIP generates higher concentrations of oxidized species near the cathode, increasing the ratio of oxidized to reduced species and, therefore, making the Nernstian potential at the cathode more positive. Consistent with this reason, the photopotential

https://dx.doi.org/10.1021/acsabm.0c00446
ACS Appl. Bio Mater. 2020, 3, 4465−4473

increases in the presence of PSI, raising the total photovoltage of the cell by 0.05 to 0.41 V, a 7-fold increase in the ratio of oxidized to reduced species for the devices measured at lower pH, and by 0.07 to 0.45 V, an 18.5-fold increase in the ratio for the devices measured at neutral pH. These large increases in the ratio of species are possible because of the ultralow concentration of oxidized species in the AscH/DCPIP system prior to light exposure and the localization of PSI on the cathode. The greater increase in photovoltage for the devices at neutral pH is attributed to D^- reacting slower with AscH than DH does at low pH, so the oxidized species generated by PSI are not consumed as rapidly, increasing the ratio of oxidized to reduced species at the cathode.[43,45]

Devices at low pH were linked in series to increase the total photovoltage (Figure 3b). The PSI-integrated devices exhibit a linear increase in photovoltage of up to 2.1 V for five devices in series as compared to 1.5 V for the devices without PSI. The photovoltage enhancement with PSI becomes important in scaling-up device fabrication because fewer materials would be needed.

PCA was used to determine how the PSI film affects the photocurrent generation at various AscH/DCPIP mediator concentrations. Figure 4 shows representative PCA curves for

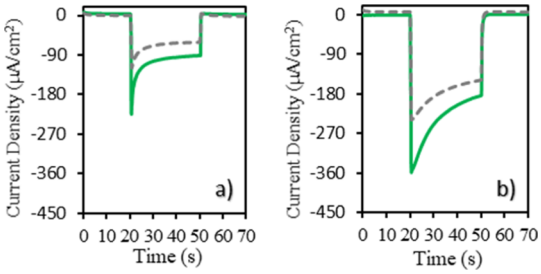

Figure 4. Photocurrent response for devices at low (a) and neutral (b) pH values with (solid green line) and without (dashed gray line) a PSI film on the copper cathode in the agarose gel with 100 mM KCl and 20 mM AscH:1 mM DCPIP. Devices were illuminated from 20 to 50 s.

devices at low and neutral pH values at a concentration of 20 mM AscH:1 mM DCPIP. The current densities for all devices follow a Cottrell-like decay under illumination, consistent with diffusional limitations for the gel devices that are similar to those observed in two- and three-electrode liquid-based PSI systems.[32,37] At both low and neutral pH values, the peak photocurrent density and the pseudo-steady state photocurrent density (after 30 s of illumination) are higher in the presence of PSI at this mediator concentration. The diffusional decay is stronger at lower pH, which is likely because of the faster consumption of oxidized DCPIP species by AscH.[49] The devices at neutral pH outperformed those at low pH, suggesting that the D^- form performs better in this system than DH, likely because DH reacts faster with AscH and slower with the P_{700} site and copper. Cyclic voltammetry of DCPIP in various pH environments showed higher electrochemical activity near neutral pH compared to acidic pH (Figure S5).

Figure 5 shows the trend between pseudo-steady photocurrent and mediator concentration for all devices. Without PSI, the pseudo-steady photocurrent density increases as concentration increases. For all concentrations, the devices near neutral pH outperform those at low pH. The pH-induced change in performance is also observed in the devices with a

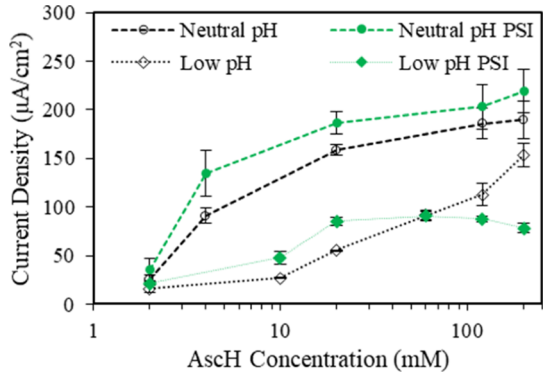

Figure 5. Steady-state photocurrent density of devices at low and neutral pH values with and without a PSI multilayer. Values were measured after 30 s of illumination for each device. For each data point, the initial ratio of AscH to DCPIP concentrations is 20:1.

PSI film on the cathode. At neutral pH, the presence of a PSI film contributes a 18−49% enhancement to photocurrent at intermediate concentrations but yields statistically similar photocurrents at high concentrations. Devices containing PSI at low pH and ranging from 2 to 20 mM AscH all showed improvements over the non-PSI devices. At 60 mM, the performance was similar, but at higher concentrations, the photocurrent density was well below that of the non-PSI devices. In all cases, photovoltage was still enhanced by 50−75 mV with PSI.

As the mediator concentration increases, the finite number of PSI reaction sites effectively becomes the limiting reagent in the production of O, and thus, the photocurrent in the presence of PSI begins to plateau. Saturation of PSI sites via Michaelis−Menten processes at high mediator concentration has also been attributed to such plateaus.[37,49] At low pH values, the devices with the PSI plateau near 90 $\mu A/cm^2$ at a concentration of 20 mM AscH and above while the neutral pH devices appear to begin plateauing above 20 mM AscH at a value ~200 $\mu A/cm^2$. The difference in the plateaus with pH is attributed to the slower reaction of D^- with AscH that yields higher concentration of oxidized species near the cathode, in addition to the increased electrochemical activity of D^-.

The devices at neutral pH outperformed those at low pH, so power curves of devices at neutral pH were produced to measure the power output with and without PSI (Figure 6a). The power curves were obtained by taking the average of $j-V$ curves done at forward and reverse scan directions to find the voltage where maximum power occurs. The forward and reverse scans (Figure S6) differ because of an imbalance of charge extraction at the electrodes, whereas the average is more representative of actual device performance.[50] Then, a steady-state power value was determined by measuring power output under illumination while devices were biased at the maximum power voltages until the steady state was reached to yield accurate power performance (Figure 6b).[51,52] Devices at 20 mM AscH:1 mM DCPIP with and without PSI showed a maximum power output of 0.033 and 0.023 mW/cm^2 and power conversion efficiencies of 0.042 and 0.028%, respectively. Table 1 shows the characteristic parameters for the $j-V$ curves obtained from forward and reverse scans as well as the average values. Instantaneous power outputs were also measured by measuring a reverse-scan $j-V$ curve at 10 V/s. The instantaneous maximum power output and efficiencies

https://dx.doi.org/10.1021/acsabm.0c00446
ACS Appl. Bio Mater. 2020, 3, 4465−4473

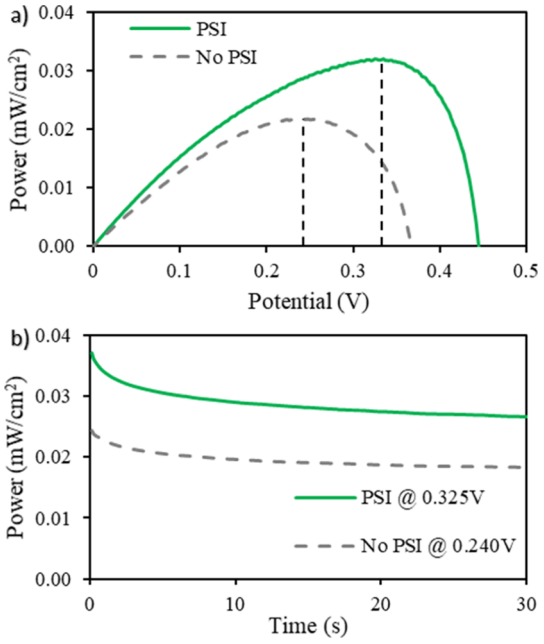

Figure 6. (a) Power curves of devices at neutral pH and a concentration of 20 mM AscH to 1 mM DCPIP. The resulting power curve represents an average of forward and reverse $j-V$ scans at 1 V/s. Light intensity (80 mW/cm^2) was used, and scans were run after 30 s of illumination. (b) Steady-state power generation of devices biased at the voltage where maximum power occurs.

Table 1. Power Parameters: Fill Factor (FF), Current Density (J_{sc}), Open Circuit Voltage (V_{oc}), and Power Conversion Efficiency (η)

	FF	J_{SC} (μA/cm^2)	V_{OC} (V)	η (%)
PSI_{Rev}	0.60	190.4	0.450	0.064
PSI_{For}	0.26	159.4	0.436	0.023
PSI_{Avg}	0.43	174.9	0.443	0.042
No PSI_{Rev}	0.47	170.9	0.375	0.037
No PSI_{For}	0.37	118.6	0.350	0.019
No PSI_{Avg}	0.42	144.8	0.363	0.028

with and without PSI were 0.24 and 0.14 mW/cm^2 and 0.30 and 0.18%, respectively (Figure S7).

To confirm that the decreased performance of the devices at low pH was because of pH and not the supporting electrolyte, replicate devices at low pH were fabricated using sodium nitrate as the supporting electrolyte, and the performance was the same as those in KCl. Additionally, devices at neutral pH with a KCl supporting electrolyte were tested and performed similarly to those with phosphate electrolyte. Phosphate is the preferred supporting electrolyte because it is stable, acts as a buffer around neutral pH values, and is not corrosive toward the copper cathode.

The presence of the relatively thick, 4 μm PSI film raised concern that a barrier effect might cause changes in performance. To confirm that the redox capabilities of PSI were causing the enhancements, devices with varying film thicknesses were fabricated by diluting the initial PSI suspension (Figure 7). Additionally, devices at low pH with a 4 μm film of deactivated PSI (thermally deactivated by boiling for 2 min) were also made to test the barrier properties of the PSI film. PSI multilayer films increased device performance with an increase in the thickness of the protein

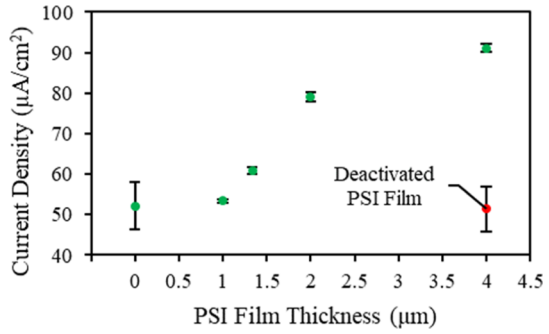

Figure 7. Effect of PSI film thickness on device performance for 20 mM AscH:1 mM DCPIP at low pH. The deactivated data were collected by thermally denaturing PSI by boiling for 10 min before deposition. The photovoltage of the cell with the deactivated film of PSI is 0.35 V, which is the same as that of the cell without PSI (0.35 V).

film by multiple deposition steps up to 2.5 μm because of the availability of more active sites in the protein film for the conversion of mediator.[7] Here, the performance continues to increase with thickness, but beyond a thickness of 2 μm, the rate of increase slows, likely caused by the film becoming thick enough that light is unable to penetrate completely through it. Additionally, the device with the deactivated 4 μm thick protein film yields the same photocurrent density and photovoltage as the devices without PSI, indicating that the performance enhancements provided by PSI are not dictated by barrier or partitioning effects. This conclusion is also confirmed by electrochemical impedance spectroscopy (EIS) because the presence of a PSI film does not significantly affect transfer of ions to the electrode (Figure S8). Collectively, these results support the conclusion that the observed enhancements in photocurrent and photovoltage are driven by PSI-mediator reactions.

Model Analysis. The reaction-diffusion system was modeled via Matlab using the *pdepe* and *lsqcurvefit* functions to solve the system of PDE's and apply the method of least squares, respectively (see Supporting Information). The model was used to estimate photocurrent density after 30 s of illumination in devices at neutral pH with and without PSI. The resulting photocurrent densities were then normalized to the photocurrent density computed for a device without PSI at the same mediator concentration of 200 mM AscH to 10 mM DCPIP to compare the model to the experimental system (Figure 8).

Two of the parameters were unknown while formulating the model: the initial ratio of O to R concentrations (C_O^*/C_R^*) and the reaction rate constant for PSI (k_{PSI}). To find these parameters, the lsqcurvefit function was used to first match the model to experimental data without PSI to obtain the initial C_O^*/C_R^* ratio. A value of 1.07×10^{-4} represents an initial conversion of ~99.99%, which is expected as the reaction of AscH with DCPIP is generally considered to approach completion.[45,53] A 99.99% conversion results in an ultralow initial concentration of O, allowing for PSI to provide a large (e.g., 18.5-fold) increase in the surface concentration ratios as seen by the photovoltage enhancements.

The value for the net rate of conversion of R to O by PSI (k_{PSI}) was determined by using *lsqcurvefit* to match the model to the experimental data with PSI, using the initial ratio of C_O^*/C_R^* obtained by modeling the experimental data without PSI.

https://dx.doi.org/10.1021/acsabm.0c00446
ACS Appl. Bio Mater. 2020, 3, 4465−4473

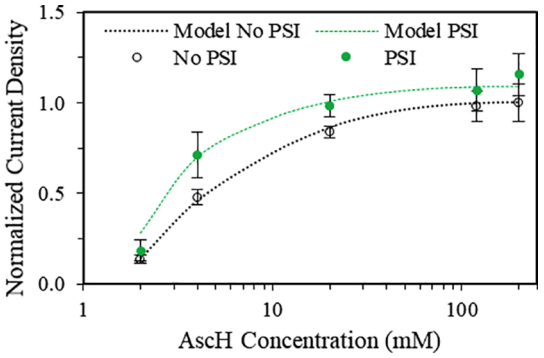

Figure 8. Comparison of model predictions (lines) for photocurrent density to experimental data (points) with PSI (filled points) and without PSI (open points) in devices at neutral pH. Values were normalized to the photocurrent density value of a device without PSI at a mediator concentration of 200 mM AscH to 10 mM DCPIP.

The first-order rate constant was fit to be 1.98×10^{-5} s^{-1}, showing that a positive net reaction rate for the production of O does result in improved photocurrent performance compared to non-PSI devices. Additionally, the model shows that if the net kinetic rate of conversion by PSI remains constant, a plateauing effect on photocurrent occurs as concentration increases, confirming that the reaction sites provided by PSI do indeed become a limiting reagent.

CONCLUSIONS

A low-cost, renewable, and gel-based biophotovoltaic device was designed and easily fabricated in this study. The device uses abundant, environmentally friendly, and inexpensive materials, including PSI, copper, TiO_2, blackberry dye, AscH, DCPIP, and agarose. The use of an agarose hydrogel enables redox reactions to occur as in a liquid device while allowing simpler construction of a two-electrode device. Within the tested concentration range, photovoltage was independent of total mediator concentration, but devices at neutral pH outperformed those at lower pH because of the pH-dependent nature of the AscH/DCPIP couple. A 4 μm thick PSI film increased photovoltage at low and neutral pH values by 50 and 75 mV, respectively, compared to devices without PSI to achieve values of up to 450 mV. Devices connected in series showed a linear increase in photovoltage with each device.

Photocurrent was dependent on mediator concentration, pH, and the presence of PSI. At both low and neutral pH values, PSI enhanced photocurrent at low to moderate mediator concentrations as compared to devices without PSI, but enhancement diminished as mediator concentration increased because of the limiting reaction capabilities of the PSI films. $j-V$ power curves obtained at neutral pH with 20 mM AscH to 1 mM DCPIP concentration showed that PSI devices had a power conversion efficiency of 0.042% compared to 0.028% without PSI. Additionally, a numerical model was developed to examine the effect of PSI-mediator oxidation kinetics on photocurrent. The model is consistent with experiments, showing that the net reaction rate of the production of O species by PSI leads to photocurrent enhancements that are more dramatic at low and intermediate concentrations of mediator.

This investigation is the first to incorporate PSI in a two-electrode gel-based cell, showing that the asymmetric redox kinetics of the protein provides enhancement to both photocurrent and photovoltage when deposited on the cathode of a DSSC. The reported devices are environmentally friendly and made from easily sourced materials with low energy input compared to many other photovoltaic technologies.

EXPERIMENTAL SECTION

Materials. PSI used in this experiment was extracted from spinach purchased at a local market. Blackberries were also purchased from a local market. Redox mediators, (AscH and DCPIP), Triton X-100 surfactant, hydroxyapatite, TiO_2 paste (Dyesol 18NR-T), and supporting electrolytes (KCl and NaH_2PO_4) were all purchased from Millipore-Sigma. 10,000 MWCO dialysis tubing (Spectrapore) was purchased from VWR. Fluorine-doped tin-oxide (FTO) substrates (TEC15) were purchased from MTI Corporation. Minibinder clips (Staples) were used for device fabrication.

PSI Extraction. PSI was extracted from commercially available spinach following steps described in previous work.[54] In short, the spinach was deveined, macerated, filtered, and then centrifuged at 8000*g* to isolate the thylakoid membranes. The supernatant was then mixed with a surfactant (Triton-X100) to lyse the membranes before the second centrifugation at 20,000*g*. A hydroxyapatite column was used to isolate the PSI. The protein was dialyzed for 24 h using 10,000 MWCO dialysis tubing to remove salts and surfactants.

FTO/TiO_2 Electrode Preparation and Dye Sensitization. FTO substrates were rinsed with ethanol and dried under a stream of nitrogen. The substrates were then treated with ozone plasma under vacuum for 15 min to create a hydrophilic surface. TiO_2 paste (Dyesol 18NR-T) was mixed in a 1:3 (v/v) ethanol solution and spin-coated onto FTO at 1500 rpm for 30 s. The films were then sintered at 500 °C in a muffle furnace for 30 min and cooled overnight.

To dye sensitize the TiO_2 substrate, 20 g of commercially available blackberries was crushed in a mortar by pestle and mixed with 20 mL of ethanol. Solids were filtered from the mixture, and the TiO_2 films were left in the dye solution for 12 h.[25] The dyed films were rinsed in ethanol and dried under nitrogen before use.

Gel Electrolyte Preparation. Aqueous-based electrolyte solutions of AscH and DCPIP (in a ratio of 20 mM AscH to 1 mM DCPIP) were used with AscH concentrations ranging from 2 to 200 mM. For devices at lower pH, 100 mM KCl served as the supporting electrolyte while at neutral pH, 100 mM monobasic phosphate was the electrolyte. Agarose was added to each liquid electrolyte at 0.5 wt % and then stirred and heated to 120 °C. The media were cooled and formed an electrolyte gel.

PSI Deposition and Device Fabrication. Copper tape was pressed onto FTO and used as the metal cathode. An insulating mask with a 0.28 cm^2 hole was placed over the copper, and a duplicate mask was placed on TiO_2, and 50 μL of 4 μM dialyzed PSI was drop-cast onto the copper into the hole made by the mask. The PSI was then dried under vacuum for 30 min, leaving a multilayer film of randomly oriented PSI protein complexes. The thickness of the protein film was measured by profilometry (Dektak). The average thickness of the multilayer films was 4 μm, which is roughly 400 layers of protein assuming a height of 10 nm/layer based on the dimensions of PSI.

Agarose gel (100 μL) was placed within the opening of the mask on the metal substrate, with or without a PSI multilayer previously deposited. The FTO slide with the TiO_2 was then pressed on top of the cathode and bound with binder clips to form the device. The average distance between the cathode and electrode was measured to be 400 μm. PM-IRRAS performed with Bruker Tensor 27 FTIR at 1 cm^{-1} resolution was used to confirm that PSI was deposited on the substrate.

Photoelectrochemical Measurements. Electrochemical characterization was performed using a CH Instruments CH660a workstation equipped with a Faraday cage. Experiments were performed using the cathode as the working electrode and TiO_2-coated FTO as the anode and reference electrodes.

All photochronoamperometric measurements were performed at a 0 V bias. Each sample was illuminated for 30 s using a 250 W cold light source (Leica KL 2500 LCD), which emitted a light intensity of

https://dx.doi.org/10.1021/acsabm.0c00446
ACS Appl. Bio Mater. 2020, 3, 4465−4473

80 mW/cm^2 at a spectral range of 380−790 nm. All measurements were normalized to the 0.28 cm^2 area made with the mask. The back side of the FTO-coated slide was illuminated so that light would penetrate the FTO/TiO_2 layers and the gel before striking the reflective cathode.

Cyclic voltammograms were obtained with an Ag/AgCl reference and a Pt counter electrode in either 100 mM phosphate buffer or KCl. A scan rate of 0.1 V/s was used for all experiments.

$j-V$ curves were produced via linear sweep voltammetry at a scan rate of 1 V/s. Scans were made in both forward and reverse directions. Scans were done after 30 s of illumination to reduce diffusional effects. Steady-state power output was determined by measuring photocurrent while the devices were biased at the voltage, where maximum power occurred on the $j-V$ curves for each device.

PSI Model. We developed a simplified electrochemical reaction-diffusion model in Matlab. The model examined the change in concentration of oxidized and reduced species as well as photocurrent density during 30 s of illumination. Values after 30 s of illumination were taken as the pseudo-steady state for the device. Devices with and without a 4 μm-thick PSI film were modeled to investigate the function of PSI in the system at various mediator concentrations.

The assumptions made for this simplified model are that the cathode is limiting the current and therefore is where heterogeneous electrode kinetics are modeled, the initial ratio of O to R is the same with or without PSI for each initial total concentration, the diffusion coefficients for O and R are the same, the diffusion coefficients for DCPIP and AscH in 0.5% agarose gel are 35% of their diffusion coefficients in liquid water, 0.77×10^{-9} and 0.87×10^{-9} m^2 s^{-1}, respectively,[55,56] the charge transfer coefficient for the DCPIP mediator is 0.5, the potential of the rate-determining step for DCPIP is 0.217 V versus SHE, the exchange current is based on a single-electron transfer taken as the rate-determining step of the two-electron DCPIP reaction, the PSI multilayer acts as redox film and does not partition concentrations, and AscH does not react at the cathode. Values for variables and constants are shown in Table 2.

Table 2. Variables and Constants Used in the Reaction-Diffusion Model

parameter	Value	units	source
C^*_{Tot}	2−200	mM	model
C^*_O/C^*_R	1.07×10^{-4}		fit
C^*_O	$C^*_O/C^*_R \times C^*_{Tot}/20$	mM	model
C^*_R	$(1 - C^*_O/C^*_R) \times C^*_{Tot}/20$	mM	model
C^*_{Asc}	$C_{Tot} - C^*_O - C^*_R$	mM	model
D_o and D_R	270	μm^2/s	55,56
D_{Asc}	310	μm^2/s	55,56
N	2	e$^-$	
A	0.5		
F	0.0257	V	
E_{metal}	0.34	V vs SHE	42
E_{DCPIP}	0.217	V vs SHE	CV
k_{PSI}	1.98×10^{-5}	s^{-1}	fit
k_{Asc}	2.99×10^{-1}	mM^{-1} s^{-1}	45
j_0	0.19 with PSI	μA/cm^2	EIS
	0.28 without PSI		

Bulk Gel. AscH reactions occur homogeneously throughout the device with and without PSI. The equations are

$$\frac{\partial C_O}{\partial t} = D_O \frac{\partial^2 C_O}{\partial x^2} - k_{Asc} C_O C_{Asc} \quad (2)$$

$$\frac{\partial C_R}{\partial t} = D_R \frac{\partial^2 C_R}{\partial x^2} + k_{Asc} C_O C_{Asc} \quad (3)$$

$$\frac{\partial C_{Asc}}{\partial t} = D_{Asc} \frac{\partial^2 C_{Asc}}{\partial x^2} - k_{Asc} C_O C_{Asc} \quad (4)$$

where $C_i(x,t)$ is the concentration of mediator, O = oxidized [DCPIP], R = reduced [$DCPIPH_2$], and Asc = [AscH] at distance x and time t, D_i is the diffusion coefficient of mediator i, and k_{Asc} is the reaction rate of AscH with O. The equations are solved for x = 0 to x = 400 μm in the absence of a PSI film and for x = 4 to x = 400 μm with a PSI film, as eqs 5−7 below accounts for the reaction when PSI is present.

PSI Film. When a 4 μm thick film is present, PSI reacts with O and R, but the kinetic asymmetry of PSI produces more O species throughout the film. The equations are

$$\frac{\partial C_O}{\partial t} = D_O \frac{\partial^2 C_O}{\partial x^2} + k_{PSI} C_R - k_{Asc} C_O C_{Asc} \quad (5)$$

$$\frac{\partial C_R}{\partial t} = D_R \frac{\partial^2 C_R}{\partial x^2} - k_{PSI} C_R + k_{Asc} C_O C_{Asc} \quad (6)$$

$$\frac{\partial C_{Asc}}{\partial t} = D_{Asc} \frac{\partial^2 C_{Asc}}{\partial x^2} - k_{Asc} C_O C_{Asc} \quad (7)$$

where k_{PSI} is the net reaction rate of PSI converting O to R. When a PSI film is present, the PSI film is treated as a homogeneous redox active film. The unknown parameter k_{PSI} was fit to match the model with a PSI film being present. The value for k_{PSI} was found by using the method of least squares fitting to experimental data with PSI.

Initial and Boundary Conditions. O, R, and AscH are all initially present, and the concentrations are assumed to be the same across the device resulting in the initial condition

$$C_i(x, 0) = C_i^* \quad (8)$$

where $C_i(x,0)$ is the concentration at t = 0, and C_i^* is the initial concentration of i. The initial ratio of O to R was found by using the method of least squares to fit the model to experimental data without PSI.

The fluxes of O and R at the electrodes are related to the current (j_{cell}) flowing through the cell by the following boundary conditions

$$j_{cell} = nFD_O \frac{dC_O}{dx}\Big|_{x=0} \qquad -j_{cell} = nFD_O \frac{dC_O}{dx}\Big|_{x=400} \quad (9)$$

$$-j_{cell} = nFD_R \frac{dC_R}{dx}\Big|_{x=0} \qquad j_{cell} = nFD_R \frac{dC_R}{dx}\Big|_{x=400} \quad (10)$$

where n is the number of electrons transferred, and F is Faraday's constant. For both O and R, the fluxes are opposite to each other at both boundaries to maintain charge balance within the cell.

AscH is assumed to not be redox active at the electrodes leading to the boundary conditions

$$0 = \frac{dC_{Asc}}{dx}\Big|_{x=0} \qquad 0 = \frac{dC_{Asc}}{dx}\Big|_{x=400} \quad (11)$$

Heterogeneous Electrode Kinetics. At the cathode and anode, the surface concentrations of the species are related to current through Butler−Volmer electrode kinetics for a rate-determining electron process[42,57]

$$j_{cell} = j_0 \times [e^{-\alpha f\eta} - e^{(1-\alpha)f\eta}] \quad (12)$$

$$\eta = E_{copper} - E_{DCPIP} + \frac{RT}{nF} \ln \frac{C_O(0, t)}{C_R(0, t)} \quad (13)$$

where j_o is the exchange current density, α is the charge transfer coefficient, η is the overpotential, E_{copper} is the potential of the copper electrode, E_{DCPIP} is the $E_{1/2}$ for DCPIP, and $C_i(0,t)$ is the surface concentration of i.

https://dx.doi.org/10.1021/acsabm.0c00446
ACS Appl. Bio Mater. 2020, 3, 4465−4473

■ ASSOCIATED CONTENT

Supporting Information

The Supporting Information is available free of charge at https://pubs.acs.org/doi/10.1021/acsabm.0c00446.

Profilometry, PM-IRRAS, CV, *j*−*V*, and EIS experiments as well as more detail on mediator selection (PDF)

■ AUTHOR INFORMATION

Corresponding Author

G. Kane Jennings − *Department of Chemical and Biomolecular Engineering, Vanderbilt University, Nashville, Tennessee 37235, United States;* orcid.org/0000-0002-3531-7388; Email: kane.g.jennings@vanderbilt.edu

Authors

Joshua M. Passantino − *Department of Chemical and Biomolecular Engineering, Vanderbilt University, Nashville, Tennessee 37235, United States;* orcid.org/0000-0002-4707-6016

Kody D. Wolfe − *Interdisciplinary Materials Science Program, Vanderbilt University, Nashville, Tennessee 37235, United States;* orcid.org/0000-0002-6452-0107

Keiann T. Simon − *Department of Chemical and Biomolecular Engineering, Vanderbilt University, Nashville, Tennessee 37235, United States*

David E. Cliffel − *Department of Chemistry, Vanderbilt University, Nashville, Tennessee 37235, United States;* orcid.org/0000-0001-8756-106X

Complete contact information is available at: https://pubs.acs.org/10.1021/acsabm.0c00446

Funding

We gratefully acknowledge support from the National Science Foundation (DMR-1507505 and 156014) and the U.S. Department of Agriculture (2019-67021-29857) for providing funding that was used by all the authors of this manuscript. The author 1 received funding from the NSF Graduate Research Fellowship Program (DGE-1445197 and DGE-1937963).

Notes

The authors declare no competing financial interest.

■ ACKNOWLEDGMENTS

We acknowledge support from the Vanderbilt Institute of Nanoscale Science and Engineering (VINSE) for use of their characterization tools and technical support.

■ ABBREVIATIONS

PSI, photosystem I; DSSC, dye-sensitized solar cell; AscH, ascorbic acid; DCPIP, 2,6-dichlorophenolindophenol; MV, methyl viologen; PM-IRRAS, polarization modulation infrared reflection−absorption spectroscopy; CV, cyclic voltammetry; EIS, electrochemical impedance spectroscopy

■ REFERENCES

(1) Grant, C. A.; Hicks, A. L. Effect of Manufacturing and Installation Location on Environmental Impact Payback Time of Solar Power. *Clean Technol. Environ. Policy* **2019**, *22*, 187.

(2) Kandilli, C. A Comparative Study on the Energetic-Exergetic and Economical Performance of a Photovoltaic Thermal System (PVT). *Res. Eng. Struct. Mater.* **2019**, *5*, 75−89.

(3) LaVan, D. A.; Cha, J. N. Approaches for Biological and Biomimetic Energy Conversion. *Proc. Natl. Acad. Sci. U.S.A.* **2006**, *103*, 5251−5255.

(4) Nelson, N.; Yocum, C. F. Structure and Function of Photosystems I and II. *Annu. Rev. Plant Biol.* **2006**, *57*, 521−565.

(5) Yu, D.; Wang, M.; Zhu, G.; Ge, B.; Liu, S.; Huang, F. Enhanced Photocurrent Production by Bio-Dyes of Photosynthetic Macromolecules on Designed TiO_2 Film. *Sci. Rep.* **2015**, *5*, 9375.

(6) Frolov, L.; Wilner, O.; Carmeli, C.; Carmeli, I. Fabrication of Oriented Multilayers of Photosystem I Proteins on Solid Surfaces by Auto-Metallization. *Adv. Mater.* **2008**, *20*, 263−266.

(7) Ciesielski, P. N.; Faulkner, C. J.; Irwin, M. T.; Gregory, J. M.; Tolk, N. H.; Cliffel, D. E.; Jennings, G. K. Enhanced Photocurrent Production by Photosystem I Multilayer Assemblies. *Adv. Funct. Mater.* **2010**, *20*, 4048−4054.

(8) Heifler, O.; Carmeli, C.; Carmeli, I. Enhanced Optoelectronics by Oriented Multilayers of Photosystem I Proteins in Dry Hybrid Bio-Solid Devices. *J. Phys. Chem. C* **2018**, *122*, 11550−11556.

(9) Baker, D. R.; Simmerman, R. F.; Sumner, J. J.; Bruce, B. D.; Lundgren, C. A. Photoelectrochemistry of Photosystem I Bound in Nafion. *Langmuir* **2014**, *30*, 13650−13655.

(10) LeBlanc, G.; Gizzie, E.; Yang, S.; Cliffel, D. E.; Jennings, G. K. Photosystem I Protein Films at Electrode Surfaces for Solar Energy Conversion. *Langmuir* **2014**, *30*, 10990−11001.

(11) Chen, W.-L.; Gross, E. L.; Pan, R. L. A Photoelectrochemical Cell Using Electrodes Modified by Photosystem I Particles of Spinach. *Bot. Bull. Acad. Sin.* **1991**, *33*, 9−15.

(12) Nguyen, K.; Bruce, B. D. Growing Green Electricity: Progress and Strategies for Use of Photosystem I for Sustainable Photovoltaic Energy Conversion. *Biochim. Biophys. Acta, Bioenerg.* **2014**, *1837*, 1553−1566.

(13) Musazade, E.; Voloshin, R.; Brady, N.; Mondal, J.; Atashova, S.; Zharmukhamedov, S. K.; Huseynova, I.; Ramakrishna, S.; Najafpour, M. M.; Shen, J.-R.; Bruce, B. D.; Allakhverdiev, S. I. Biohybrid Solar Cells: Fundamentals, Progress, and Challenges. *J. Photochem. Photobiol., C* **2018**, *35*, 134−156.

(14) Das, R.; Kiley, P. J.; Segal, M.; Norville, J.; Yu, A. A.; Wang, L.; Trammell, S. A.; Reddick, L. E.; Kumar, R.; Stellacci, F.; Lebedev, N.; Schnur, J.; Bruce, B. D.; Zhang, S.; Baldo, M. Integration of Photosynthetic Protein Molecular Complexes in Solid-State Electronic Devices. *Nano Lett.* **2004**, *4*, 1079−1083.

(15) Gordiichuk, P. I.; Wetzelaer, G.-J. A. H.; Rimmerman, D.; Gruszka, A.; De Vries, J. W.; Saller, M.; Gautier, D. A.; Catarci, S.; Pesce, D.; Richter, S.; Blom, P. W. M.; Herrmann, A. Solid-State Biophotovoltaic Cells Containing Photosystem I. *Adv. Mater.* **2014**, *26*, 4863−4869.

(16) Gizzie, E. A.; Scott Niezgoda, J.; Robinson, M. T.; Harris, A. G.; Jennings, G. K.; Rosenthal, S. J.; Cliffel, D. E. Photosystem I-Polyaniline/TiO_2 Solid-State Solar Cells: Simple Devices for Biohybrid Solar Energy Conversion. *Energy Environ. Sci.* **2015**, *8*, 3572−3576.

(17) Olmos, J. D. J.; Becquet, P.; Gront, D.; Sar, J.; Dąbrowski, A.; Gawlik, G.; Teodorczyk, M.; Pawlak, D.; Kargul, J. Biofunctionalisation of P-Doped Silicon with Cytochrome c_{553} Minimises Charge Recombination and Enhances Photovoltaic Performance of the All-Solid-State Photosystem I-Based Biophotoelectrode. *RSC Adv.* **2017**, *7*, 47854−47866.

(18) Zeynali, A.; Ghiasi, T. S.; Riazi, G.; Ajeian, R. Organic Solar Cell Based on Photosystem I Pigment-Protein Complex, Fabrication and Optimization. *Org. Electron. physics, Mater. Appl.* **2017**, *51*, 341−348.

(19) Kazemzadeh, S.; Riazi, G.; Ajeian, R. Novel Approach of Biophotovoltaic Solid State Solar Cells Based on a Multilayer of PS1 Complexes as an Active Layer. *ACS Sustain. Chem. Eng.* **2017**, *5*, 9836−9840.

(20) Dervishogullari, D.; Gizzie, E. A.; Jennings, G. K.; Cliffel, D. E. Polyviologen as Electron Transport Material in Photosystem I-Based Biophotovoltaic Cells. *Langmuir* **2018**, *34*, 15658−15664.

(21) Wolfe, K. D.; Dervishogullari, D.; Stachurski, C. D.; Passantino, J. M.; Jennings, G. K.; Cliffel, D. E. Photosystem I Multilayers within Porous Indium Tin Oxide Cathodes Enhance Mediated Electron Transfer. *ChemElectroChem* **2019**, *7*, 596.
(22) Ye, M.; Wen, X.; Wang, M.; Iocozzia, J.; Zhang, N.; Lin, C.; Lin, Z. Recent Advances in Dye-Sensitized Solar Cells: From Photoanodes, Sensitizers and Electrolytes to Counter Electrodes. *Mater. Today* **2015**, *18*, 155−162.
(23) Xiang, W.; Huang, F.; Cheng, Y.-B.; Bach, U.; Spiccia, L. Aqueous Dye-Sensitized Solar Cell Electrolytes Based on the Cobalt(II)/(III) Tris(Bipyridine) Redox Couple. *Energy Environ. Sci.* **2013**, *6*, 121−127.
(24) Mershin, A.; Matsumoto, K.; Kaiser, L.; Yu, D.; Vaughn, M.; Nazeeruddin, M. K.; Bruce, B. D.; Graetzel, M.; Zhang, S. Self-Assembled Photosystem-I Biophotovoltaics on Nanostructured TiO_2 and ZnO. *Sci. Rep.* **2012**, *2*, 234.
(25) Robinson, M. T.; Armbruster, M. E.; Gargye, A.; Cliffel, D. E.; Jennings, G. K. Photosystem I Multilayer Films for Photovoltage Enhancement in Natural Dye-Sensitized Solar Cells. *ACS Appl. Energy Mater.* **2018**, *1*, 301−305.
(26) Qiu, X.; Castañeda Ocampo, O.; De Vries, H. W.; Van Putten, M.; Loznik, M.; Herrmann, A.; Chiechi, R. C. Self-Regenerating Soft Biophotovoltaic Devices. *ACS Appl. Mater. Interfaces* **2018**, *10*, 37625−37633.
(27) Ciesielski, P. N.; Hijazi, F. M.; Scott, A. M.; Faulkner, C. J.; Beard, L.; Emmett, K.; Rosenthal, S. J.; Cliffel, D.; Jennings, G. K. Photosystem I-Based Biohybrid Photoelectrochemical Cells. *Bioresour. Technol.* **2010**, *101*, 3047−3053.
(28) Grätzel, M. Dye-Sensitized Solar Cells. *J. Photochem. Photobiol., C* **2003**, *4*, 145−153.
(29) Tsai, C.-H.; Lu, C.-Y.; Chen, M.-C.; Huang, T.-W.; Wu, C.-C.; Chung, Y.-W. Efficient Gel-State Dye-Sensitized Solar Cells Adopting Polymer Gel Electrolyte Based on Poly(Methyl Methacrylate). *Org. Electron. Physics, Mater. Appl.* **2013**, *14*, 3131−3137.
(30) Bidikoudi, M.; Perganti, D.; Karagianni, C.-S.; Falaras, P. Solidification of Ionic Liquid Redox Electrolytes Using Agarose Biopolymer for Highly Performing Dye-Sensitized Solar Cells. *Electrochim. Acta* **2015**, *179*, 228−236.
(31) Wang, W.; Guo, X.; Yang, Y. Lithium Iodide Effect on the Electrochemical Behavior of Agarose Based Polymer Electrolyte for Dye-Sensitized Solar Cell. *Electrochim. Acta* **2011**, *56*, 7347−7351.
(32) Badura, A.; Guschin, D.; Kothe, T.; Kopczak, M. J.; Schuhmann, W.; Rögner, M. Photocurrent Generation by Photosystem 1 Integrated in Crosslinked Redox Hydrogels. *Energy Environ. Sci.* **2011**, *4*, 2435−2440.
(33) Bennett, T. H.; Vaughn, M. D.; Davari, S. A.; Park, K.; Mukherjee, D.; Khomami, B. Jolly Green MOF: Confinement and Photoactivation of Photosystem I in a Metal-Organic Framework. *Nanoscale Adv.* **2019**, *1*, 94.
(34) Chen, G.; LeBlanc, G.; Jennings, G. K.; Cliffel, D. E. Effect of Redox Mediator on the Photo-Induced Current of a Photosystem I Modified Electrode. *J. Electrochem. Soc.* **2013**, *160*, H315−H320.
(35) Kavan, L.; Tétreault, N.; Moehl, T.; Grätzel, M. Electrochemical Characterization of TiO_2 Blocking Layers for Dye-Sensitized Solar Cells. *J. Phys. Chem. C* **2014**, *118*, 16408−16418.
(36) Manocchi, A. K.; Baker, D. R.; Pendley, S. S.; Nguyen, K.; Hurley, M. M.; Bruce, B. D.; Sumner, J. J.; Lundgren, C. A. Photocurrent Generation from Surface Assembled Photosystem I on Alkanethiol Modified Electrodes. *Langmuir* **2013**, *29*, 2412−2419.
(37) Robinson, M. T.; Cliffel, D. E.; Jennings, G. K. An Electrochemical Reaction-Diffusion Model of the Photocatalytic Effect of Photosystem I Multilayer Films. *J. Phys. Chem. B* **2018**, *122*, 117−125.
(38) Youngblood, W. J.; Lee, S. H.; Kobayashi, Y.; Hernandez-Pagan, E. A.; Hoertz, P. G.; Moore, T. A.; Moore, A. L.; Gust, D.; Mallouk, T. E. Photoassisted Overall Water Splitting in a Visible Light-Absorbing Dye-Sensitized Photoelectrochemical Cell. *J. Am. Chem. Soc.* **2009**, *131*, 926−927.
(39) Trubitsin, B. V.; Mamedov, M. D.; Semenov, A. Y.; Tikhonov, A. N. Interaction of Ascorbate with Photosystem I. *Photosynth. Res.* **2014**, *122*, 215−231.
(40) Takagi, D.; Takumi, S.; Hashiguchi, M.; Sejima, T.; Miyake, C. Superoxide and Singlet Oxygen Produced within the Thylakoid Membranes Both Cause Photosystem I Photoinhibition. *Plant Physiol.* **2016**, *171*, 1626−1634.
(41) Vernon, L. P.; Zaugg, W. S. Photoreductions by Fresh and Aged Chloropasts: Requirement for Ascorbate and 2,6-Dichlorophenolindophenol with Aged Chloroplasts. *J. Biol. Chem.* **1960**, *235*, 2728−2733.
(42) Bard, A. J.; Faulkner, L. R. *Electrochemical Methods: Fundamentals and Applications*, 2nd ed.; John Wiley & Sons, Inc., 2001.
(43) Marchanka, A.; Gastel, M. v. Reversed Freeze Quench Method near the Solvent Phase Transition. *J. Phys. Chem. A* **2012**, *116*, 3899−3906.
(44) Petrova, A.; Mamedov, M.; Ivanov, B.; Semenov, A.; Kozuleva, M. Effect of Artificial Redox Mediators on the Photoinduced Oxygen Reduction by Photosystem I Complexes. *Photosynth. Res.* **2018**, *137*, 421−429.
(45) Tonomura, B. i.; Nakatani, H.; Ohnishi, M.; Yamaguchi-Ito, J.; Hiromi, K. Test Reactions for a Stopped Flow Apparatus. *Anal. Biochem.* **1978**, *84*, 370−383.
(46) Robinson, M. T.; Simons, C. E.; Cliffel, D. E.; Jennings, G. K. Photocatalytic Photosystem I/PEDOT Composite Films Prepared by Vapor-Phase Polymerization. *Nanoscale* **2017**, *9*, 6158−6166.
(47) Kumara, N. T. R. N.; Lim, A.; Lim, C. M.; Petra, M. I.; Ekanayake, P. Recent Progress and Utilization of Natural Pigments in Dye Sensitized Solar Cells: A Review. *Renewable Sustainable Energy Rev.* **2017**, *78*, 301−317.
(48) Ferber, J.; Stangl, R.; Luther, J. Electrical Model of the Dye-Sensitized Solar Cell. *Sol. Energy Mater. Sol. Cells* **1998**, *53*, 29−54.
(49) Buesen, D.; Hoefer, T.; Zhang, H.; Plumeré, N. A Kinetic Model for Redox-Active Film Based Biophotoelectrodes. *Faraday Discuss.* **2019**, *215*, 39.
(50) Zimmermann, I.; Gratia, P.; Martineau, D.; Grancini, G.; Audinot, J.-N.; Wirtz, T.; Nazeeruddin, M. K. Improved Efficiency and Reduced Hysteresis in Ultra-Stable Fully Printable Mesoscopic Perovskite Solar Cells through Incorporation of CuSCN into the Perovskite Layer. *J. Mater. Chem. A* **2019**, *7*, 8073−8077.
(51) Wagner, L.; Chacko, S.; Mathiazhagan, G.; Mastroianni, S.; Hinsch, A. High Photovoltage of 1 V on a Steady-State Certified Hole Transport Layer-Free Perovskite Solar Cell by a Molten-Salt Approach. *ACS Energy Lett.* **2018**, *3*, 1122−1127.
(52) Jeon, N. J.; Noh, J. H.; Yang, W. S.; Kim, Y. C.; Ryu, S.; Seo, J.; Seok, S. I. Compositional Engineering of Perovskite Materials for High-Performance Solar Cells. *Nature* **2015**, *517*, 476−480.
(53) Karayannis, M. I. Comparative Kinetic Study for Rate Constant Determination of the Reaction of Ascorbic Acid with 2,6-Dichlorophenolindophenol. *Talanta* **1976**, *23*, 27−30.
(54) Kincaid, H. A.; Niedringhaus, T.; Ciobanu, M.; Cliffel, D. E.; Jennings, G. K. Entrapment of Photosystem I within Self-Assembled Films. *Langmuir* **2006**, *22*, 8114−8120.
(55) Fradet, E.; Abbyad, P.; Vos, M. H.; Baroud, C. N. Parallel Measurements of Reaction Kinetics Using Ultralow-Volumes. *Lab Chip* **2013**, *13*, 4326−4330.
(56) Pénicaud, C.; Peyron, S.; Bohuon, P.; Gontard, N.; Guillard, V. Ascorbic Acid in Food: Development of a Rapid Analysis Technique and Application to Diffusivity Determination. *Food Res. Int.* **2010**, *43*, 838−847.
(57) Newman, J.; Thomas-Alyea, K. E. *Electrochemical Systems*. 3rd ed.; John Wiley & Sons, 2004.

https://dx.doi.org/10.1021/acsabm.0c00446
ACS Appl. Bio Mater. 2020, 3, 4465−4473